Vaccine 60 (2025) 127314

Contents lists available at ScienceDirect

Vaccine

journal homepage: www.elsevier.com/locate/vaccine

Development and characterization of MRC-5 and Vero cell-adapted enterovirus D68 strains for vaccine production

Kota Senpuku [a,b], Yuta Kunishima [b,c], Kotaro Taniguchi [a,b], Taiki Ito [b], Toshiro Hirai [a,b,d,e], Teruya Nakamura [f], Chikako Kataoka-Nakamura [c], Yasuo Yoshioka [a,b,c,d,e,g,h,*]

[a] Laboratory of Nano-design for Innovative Drug Development, Graduate School of Pharmaceutical Sciences, The University of Osaka, 1-6 Yamadaoka, Suita, Osaka 565-0871, Japan
[b] Vaccine Creation Group, BIKEN Innovative Vaccine Research Alliance Laboratories, Research Institute for Microbial Diseases, The University of Osaka, 1-6 Yamadaoka, Suita, Osaka 565-0871, Japan
[c] The Research Foundation for Microbial Diseases of Osaka University, 3-1 Yamadaoka, Suita, Osaka 565-0871, Japan
[d] Vaccine Creation Group, BIKEN Innovative Vaccine Research Alliance Laboratories, Institute for Open and Transdisciplinary Research Initiatives, The University of Osaka, 3-1 Yamadaoka, Suita, Osaka 565-0871, Japan
[e] Center for Advanced Modalities and DDS, The University of Osaka, 3-1 Yamadaoka, Suita, Osaka 565-0871, Japan
[f] Graduate School of Pharmaceutical Sciences, Kumamoto University, 5-1 Oe-honmachi, Chuo-ku, Kumamoto 862-0973, Japan
[g] Global Center for Medical Engineering and Informatics, The University of Osaka, 3-1 Yamadaoka, Suita, Osaka 565-0871, Japan
[h] Center for Infectious Disease Education and Research, The University of Osaka, 3-1 Yamadaoka, Suita, Osaka 565-0871, Japan

ARTICLE INFO

Keywords:
Enterovirus D68
Vaccine
Vaccine manufacturing
Vero cells
MRC-5 cells

ABSTRACT

Enterovirus D68 (EV-D68) is a pathogen that causes respiratory and neurological diseases. Currently, there are no licensed vaccines for EV-D68. Here, we adapted EV-D68 to MRC-5 and Vero cells, which are widely used in vaccine manufacturing, to develop EV-D68 strains applicable for vaccine production. We successfully isolated MRC-5 cell-adapted strains by serial passaging in MRC-5 cells. Although efforts to isolate Vero cell-adapted strains through serial passaging of EV-D68 in Vero cells were unsuccessful, we isolated Vero cell-adapted strains by serial passaging of MRC-5 cell-adapted strains in Vero cells. Inactivated whole-virion vaccines were prepared from vaccine-manufacturing cell-adapted strains and mice were immunized with these vaccines. We found that in some cases, the parental and cell-adapted strains induced similar levels of protective immunity against EV-D68, whereas in other cases, the cell-adapted strains were significantly less effective than the parental strains. These data provide valuable information for EV-D68 vaccine production.

1. Introduction

Enterovirus D68 (EV-D68) is a non-enveloped icosahedral virus belonging to the family Picornaviridae, genus *Enterovirus*, species *Enterovirus D*. EV-D68 has a positive-sense, single-stranded RNA genome approximately 7.4 kb in size. The polypeptide encoded in the open reading frame is post-translationally processed into four structural proteins (VP1, VP2, VP3, and VP4) and seven non-structural proteins (2 A, 2B, 2C, 3 A, 3B, 3C, and 3D) [1–3]. EV-D68 infection primarily causes mild-to-severe respiratory diseases, mostly in children. In addition, EV-D68 is associated with neurological diseases in some patients, with acute flaccid myelitis (AFM) being the most commonly reported [4–8]. EV-D68 outbreaks occurred biennially between 2014 and 2018 with a concurrent increase in the number of AFM cases reported [3,9–11]. In 2021 and 2022, there were increasing reports of severe respiratory illnesses associated with EV-D68 infection in several countries [12,13].

Abbreviations: AFM, acute flaccid myelitis; ATCC, American Type Culture Collection; BPL, β-propiolactone; CPE, cytopathic effect; cryo-EM, cryo-electron microscopy; DMEM, Dulbecco's modified Eagle's medium; ELISA, enzyme-linked immunosorbent assay; EV, Enterovirus; EV-D68, Enterovirus D68; FBS, fetal bovine serum; HRP, horseradish peroxidase; ICAM-5, intercellular adhesion molecule 5; MFSD6, major facilitator superfamily domain containing 6; MOI, multiplicity of infection; OD, optical density; PBS, phosphate-buffered saline; RD, rhabdomyosarcoma; SARS-CoV-2, severe acute respiratory syndrome coronavirus 2; SDS-PAGE, Sodium dodecyl sulfate-polyacrylamide gel electrophoresis; $TCID_{50}$, 50 % tissue culture infectious dose; TEM, transmission electron microscopy; WV, whole-virion.

* Corresponding author at: Vaccine Creation Group, BIKEN Innovative Vaccine Research Alliance Laboratories, Research Institute for Microbial Diseases, The University of Osaka, 3-1 Yamadaoka, Suita, Osaka 565-0871, Japan.
E-mail address: y-yoshioka@biken.osaka-u.ac.jp (Y. Yoshioka).

https://doi.org/10.1016/j.vaccine.2025.127314
Received 20 November 2024; Received in revised form 16 May 2025; Accepted 21 May 2025
Available online 26 May 2025

Although EV-D68 outbreaks continue to occur and remain a major threat to global health, no approved treatments or vaccines are currently available. Therefore, there is an urgent need to develop vaccines against EV-D68.

The utility of inactivated whole-virion (WV) vaccines against EV-D68 has been reported, including our previous study [14–18]. These studies demonstrated that an inactivated WV vaccine can induce EV-D68-specific neutralizing antibodies and prevent both respiratory infection and onset of limb paralysis in mice [14–18]. Inactivated WV vaccines are prepared from viruses cultured using substrates such as cultured cells [19]. Human rhabdomyosarcoma (RD) cells have been commonly used to culture EV-D68 in various experiments [20]. However, there is no history of RD cell use in the production of approved vaccines. Furthermore, RD cells have been reported to be tumorigenic in nude mice [21]. According to the World Health Organization, US Food and Drug Administration, and European Pharmacopoeia guidelines, cell substrates used in vaccine production must be subjected to tumorigenicity tests in light of safety concerns [19,22–25]. Therefore, safety concerns have hindered the use of RD cells as a substrate for vaccine production. In addition, the complexity and high cost of establishing a system to properly assess RD cell-derived impurities are barriers to the use of RD cells.

MRC-5 and Vero cells are typical cell substrates widely used for vaccine production [24]. MRC-5 cells are human lung-derived diploid cells. Diploid cell lines have been shown to be non-tumorigenic and are well characterized in terms of safety [19,24]. MRC-5 cells have been used to produce vaccines against viruses such as measles, rubella, and varicella zoster virus [20,24]. Several EV-D68 strains have demonstrated the ability to replicate in MRC-5 cells [26]. Thus, MRC-5 cells may be a useful cell substrate for the production of vaccines against EV-D68. However, a disadvantage of using MRC-5 cells is that their growth capacity declines after 20 passages. Therefore, MRC-5 cells are not always suitable for the production of inactivated WV vaccines, which require mass culture, but they are generally useful for the production of live vaccines administered at relatively low doses [24,27]. Vero cells are a continuous cell line derived from African green monkey kidney. This cell line has been used to produce vaccines such as those against poliovirus, Japanese encephalitis virus, rabies virus, severe acute respiratory syndrome coronavirus 2 (SARS-CoV-2), and rotavirus [24]. Vero cells are unable to produce type I interferons in response to viral infection, which is thought to be the main reason for their high susceptibility to various viruses [28–30]. However, Vero cells have been reported to be non-permissive to EV-D68 [31,32]. Therefore, the development of EV-D68 strains adapted to Vero cells is important for practical application of EV-D68 vaccines.

In this study, to develop EV-D68 strains applicable to vaccine production, we adapted EV-D68 to MRC-5 and Vero cells, which are widely used as vaccine-manufacturing cells. We also evaluated the efficacy of inactivated WV vaccines prepared from the cell-adapted EV-D68 strains.

2. Materials and methods

2.1. Ethics

All animal experiments were performed in accordance with the institutional guidelines of The University of Osaka for the ethical treatment of animals and were approved by the Animal Care and Use Committee of the Research Institute for Microbial Diseases, The University of Osaka, Japan (protocol number: BIKEN-AP-R01–15-3). Experiments using EV-D68 were approved by the Institutional Review Board of the Research Institute for Microbial Diseases, The University of Osaka (protocol number: BIKEN-00184-004).

2.2. Cells

RD-A cells were kindly provided by Dr. Hiroyuki Shimizu (National Institute of Infectious Diseases, Tokyo, Japan). MRC-5 and Vero cells were procured from the American Type Culture Collection (ATCC, Manassas, VA, USA). These cells were cultured in Dulbecco's modified Eagle's medium (DMEM) with high glucose content, supplemented with 1 % streptomycin, 1 % penicillin, and 10 % heat-inactivated fetal bovine serum (FBS). The cultures were maintained in a humidified incubator at 37 °C and 5 % CO_2.

2.3. Viruses

EV-D68 US/MO/14–18,947 (MO strain, clade B1), US/KY/14–18,953 (KY strain, clade D), and US/IL/14–18,952 (IL strain, clade B2) strains were procured from the ATCC. The ATCC codes for the MO, IL, and KY strains were VR-1823, VR-1824, and VR-1825, respectively. According to the ATCC, these strains were RD cell-passaged. We passaged these strains four times in RD-A cells before beginning our experiments. The viral stocks were maintained at −80 °C. Viral titers were assessed using the Karber method [33].

2.4. Mice

Six-week-old female BALB/c mice were obtained from SLC (Hamamatsu, Japan). They were housed in a controlled environment with a 12-h light-dark cycle (lights on at 8:00 a.m. and lights off at 8:00 p.m.) and provided with free access to food and water. For anesthesia, the mice were injected intraperitoneally with a mixture of 0.3 mg/kg medetomidine hydrochloride (Nippon Zenyaku Kogyo Co., Ltd., Fukushima, Japan), 4 mg/kg midazolam (Maruishi Pharmaceutical Co., Ltd., Osaka, Japan), and 5 mg/kg butorphanol tartrate (Meiji Animal Health Co., Ltd., Kumamoto, Japan). The mice were euthanized by CO_2 inhalation.

2.5. Adaptation of EV-D68 to MRC-5 and Vero cells

For the first passage, MRC-5 cells were infected with the MO strain at a multiplicity of infection (MOI) of 3, IL strain at an MOI of 10, and KY strain at an MOI of 10; then, the cells were incubated at 33 °C under 5 % CO_2. When cytopathic effects (CPE) were observed (7 days post-infection), the cells and supernatants were collected, subjected to three cycles of freezing and thawing, and centrifuged (2100 ×*g*, 10 min, 4 °C). The resulting supernatants were stored at −80 °C as viral stocks. In the second and subsequent passages, 200 μL of the virus stocks were used to infect MRC-5 cells seeded at 80 % confluence in 100-mm dishes. When CPE was observed (4–6 days post-infection), the viruses were collected. A total of five passages were performed in MRC-5 cells, and viral stocks from the fifth passage were used for the first passage in Vero cells. For passages in Vero cells, 500 μL of virus stocks were used to infect Vero cells seeded at 80 % confluence in 150-mm dishes. When CPE was observed (5–7 days post-infection), the viruses were collected. A total of 15 passages were performed in Vero cells. Viral clones were obtained from each viral stock by plaque isolation. The volume of virus used to infect the MRC-5 and Vero cells was determined based on the culture area of the dishes. The titers of representative viruses in serial passages in MRC-5 and Vero cells are shown in Table 1.

Table 1
Viral titers ($TCID_{50}$/mL) of representative viruses in serial passages.

	MO	KY	IL
Parental strain	$10^{7.5}$	$10^{8.0}$	$10^{8.0}$
MRC-P1	$10^{6.2}$	$10^{6.9}$	$10^{6.7}$
MRC-P5	$10^{6.1}$	$10^{7.7}$	$10^{6.7}$
Vero-P1	$10^{7.5}$	$10^{7.1}$	$10^{7.0}$
Vero-P5	$10^{6.9}$	$10^{7.4}$	$10^{7.0}$
Vero-P10	$10^{7.6}$	$10^{7.3}$	$10^{7.2}$
Vero-P15	$10^{8.3}$	$10^{8.3}$	$10^{8.0}$

2.6. Viral RNA sequencing

Viral RNA was extracted from each viral stock using a High Pure Viral RNA Kit (Roche, Mannheim, Germany), according to the manufacturer's protocol. Viral RNA was processed and analyzed at the Genome Information Research Center of The University of Osaka using a NovaSeq6000 (Illumina, San Diego, CA, USA). The sequences of the MO, KY, and IL strains available from GenBank were used as reference sequences. The GenBank accession numbers for the MO, KY, and IL strains are KM851225.1, KM851231.1, and KM851230.1, respectively.

2.7. Growth curves

RD-A, MRC-5, and Vero cells were seeded in 24-well plates and inoculated with the virus at an MOI of 0.1. After incubation with the virus for 1 h at 33 °C and 5 % CO_2, the inoculum was removed. The cells were then washed twice with DMEM containing 2 % FBS, then DMEM containing 2 % FBS was added, and the cells were incubated at 33 °C and 5 % CO_2. At the indicated hours post-infection, the culture plates were subjected to three cycles of freezing and thawing, followed by centrifugation (2100 ×*g*, 10 min, 4 °C). The resultant supernatant was stored at −80 °C until assay, and viral titers at each time point were determined using the 50 % tissue culture infectious dose ($TCID_{50}$) assay.

2.8. Competition assay

RD-A and Vero cells seeded into 24-well plates were inoculated with the virus at an MOI of 0.1 in the presence of 0.04, 0.2, 1, 5, or 25 mg/mL *N*-acetylneuraminic acid or heparin. After incubation with the virus for 1 h at 33 °C and 5 % CO_2, the inoculum was removed. The cells were washed twice with DMEM containing 2 % FBS, then DMEM containing 2 % FBS was added, and the cells were incubated at 33 °C and 5 % CO_2. After 3 days, the culture plates were subjected to three cycles of freezing and thawing, followed by centrifugation (2100 ×*g*, 10 min, 4 °C). The resultant supernatant was stored at −80 °C until assay, and viral titers were determined using the $TCID_{50}$ assay.

2.9. Generation of inactivated WV vaccines

RD-A, MRC-5, or Vero cells were cultured in DMEM supplemented with 10 % FBS at 37 °C until they reached approximately 80 % confluence. After removing the FBS-containing medium and washing the cells with phosphate-buffered saline (PBS), the cells were infected with EV-D68 at 33 °C in Virus Production Serum-Free Medium (Thermo Fisher Scientific, Waltham, MA, USA). Two to five days post-infection, once complete CPE was apparent, all cultures were collected and centrifuged (2100 ×*g*, 10 min, 4 °C). The supernatant was filtered through a 0.2 μm Nalgene Rapid-Flow bottle top filter (Thermo Fisher Scientific). The virus was inactivated using *β*-propiolactone (0.05 %, 1 day, 4 °C; FUJIFILM Wako Pure Chemical Corporation, Osaka, Japan). Following viral inactivation, the *β*-propiolactone was inactivated by 2-h incubation at 37 °C. The inactivated virus was purified by centrifugation using a 20 % sucrose cushion (Beckman SW32Ti rotor, 141,000 ×*g*, 3 h, 4 °C), followed by sucrose density gradient ultracentrifugation (10–40 % sucrose, Beckman SW32Ti rotor, 130,000 ×*g*, 4 h, 4 °C). Fractions containing EV-D68 full particles were identified by western blotting using an anti-VP2 antibody (catalog number: GTX132314; dilution: 1/5000; GeneTex, Irvine, CA, USA). Subsequently, the fractions were concentrated using 100 kDa molecular weight cutoff Amicon ultracentrifugal filters (Merck Millipore, Darmstadt, Germany) and resuspended in PBS. The protein concentration was measured using a BCA Protein Assay Kit (Thermo Fisher Scientific).

2.10. Sodium dodecyl sulfate-polyacrylamide gel electrophoresis (SDS-PAGE)

The inactivated WV vaccines were combined with a sample buffer solution (Nacalai Tesque, Kyoto, Japan) containing *β*-mercaptoethanol and heated at 95 °C for 5 min. They were then loaded onto a 10 % Extra PAGE One Precast Gel (Nacalai Tesque). After electrophoresis, the gel was stained with Coomassie Brilliant Blue using EzStain AQua staining solution (ATTO, Tokyo, Japan).

2.11. Western blotting

Following SDS-PAGE, protein bands were transferred onto polyvinylidene fluoride membranes (Bio-Rad, Hercules, CA, USA) and blocked using 5 % skim milk (*w/v*) diluted in PBS containing 0.05 % Tween 20 (PBS-T). Subsequently, the membrane was rinsed three times with PBS-T and incubated with rabbit polyclonal anti-EV-D68 VP2 antibody (catalog number: GTX132314; dilution: 1/5000; GeneTex). After three PBS-T washes, the membranes were treated with horseradish peroxidase (HRP)-conjugated anti-rabbit IgG antibody (catalog number: 458; dilution: 1/5000; Medical & Biological Laboratories, Tokyo, Japan) and visualized using a ChemiDoc Touch Imaging System (Bio-Rad).

2.12. Particle size measurement

Dynamic light scattering (Zetasizer Nano-ZS, Malvern Panalytical Ltd., Worcestershire, UK) was used to measure the size distribution of the inactivated WV vaccines.

2.13. Negative-stain transmission electron microscopy (TEM)

Hydrophilized carbon-formvar grids were submerged in a 20 μL sample solution of the assembly reaction for 10 min. Subsequently, the grids were rinsed with distilled water and stained using 2 % uranyl acetate. They were then dried using filter paper to remove excess moisture, left to air-dry for 30 min, and observed using an 80 kV JEOL JEM-1400plus electron microscope. Images were captured using an Olympus Veleta 2 K × 2 K side-mounted TEM charge-coupled device camera.

2.14. Vaccination

Mice were vaccinated subcutaneously with 0.1 μg inactivated WV vaccine prepared in 50 μL PBS at the base of the tail on days 0 and 21. Blood samples were drawn on days 14 and 28 and stored at −30 °C for subsequent analysis.

2.15. Detection of EV-D68-specific antibodies

The levels of EV-D68-specific IgG in the plasma were detected using an enzyme-linked immunosorbent assay (ELISA), as previously reported [18]. Briefly, a 96-well half area flat-bottom plate (Corning, NY, USA) was coated with 0.6 μg/mL purified non-inactivated EV-D68 full particles in carbonate buffer. The coated plates were then incubated with blocking solution (1 % Block Ace; DS Pharma Biomedical, Osaka, Japan) for 1 h at room temperature. Plasma samples were serially diluted before addition to the EV-D68-coated plates. After incubation for 2 h at room temperature, the plates were incubated with HRP-conjugated goat anti-mouse IgG (catalog number: 1030–05; dilution: 1/5000; SouthernBiotech, Birmingham, AL, USA) for 1 h at room temperature. The colorimetric reaction was initiated using tetramethylbenzidine, followed by termination using 2 N H_2SO_4. The difference in optical density (OD) between 450 and 570 nm ($OD_{450–570}$) was detected using a microplate reader (PowerWave HT; Bio-Tek Instruments, Inc., Winooski, VT, USA).

2.16. Neutralization assay

Neutralizing antibody titers were measured as previously reported [18]. Briefly, plasma samples were serially diluted 2-fold in DMEM containing 2 % FBS in 96-well plates after inactivation at 56 °C for 30 min. Diluted plasma samples were incubated with 100 $TCID_{50}$ EV-D68 for 1 h at 37 °C. RD-A cells were added at 1.5×10^4 cells/well and cultured at 33 °C and 5 % CO_2 for 7 days. Neutralizing antibody titers were defined as the highest plasma dilution at which CPE was completely inhibited.

2.17. Determination of viral load in tissues

Ten days after boost immunization, the mice were anesthetized and intranasally challenged with 5.0×10^6 $TCID_{50}$ of EV-D68 in a total volume of 20 μL PBS (10 μL in each nostril). Subsequently, lung and nasal turbinate samples were harvested 12 h post-challenge and placed into screw-cap tubes containing 4.0 mm stainless-steel beads (TAITEC, Saitama, Japan), followed by the addition of 500 μL DMEM. Mechanical lysis of the tissue samples was performed using a μT-12 bead crusher (TAITEC), and after the addition of another 500 μL of DMEM, the samples were centrifuged (10,000 ×*g*, 5 min, 4 °C). The viral load in the supernatant was quantified using the $TCID_{50}$ assay starting with a 100-fold dilution.

2.18. Detection of EV-D68 RNA in tissues using quantitative polymerase chain reaction (qPCR)

Total RNA was extracted from the nasal turbinates and lungs of challenged mice using TRIzol reagent (Invitrogen, Carlsbad, CA, USA). At 0, 4, 12, 24, 48, and 96 h after challenge, the nasal turbinates and lungs were collected into a tube containing 1 mL of TRIzol reagent and stainless-steel beads and crushed using a μT-12 bead crusher. After centrifugation (12,000 ×*g*, 5 min, 4 °C), 200 μL of chloroform was added to the collected supernatant, mixed, and centrifuged again (12,000 ×*g*, 5 min, 4 °C). The aqueous layer was collected, and 500 μL of isopropanol was added. After incubation at 4 °C for 10 min, the sample was centrifuged (12,000 ×*g*, 10 min, 4 °C), and the pellet was washed with 75 % ethanol. The obtained RNA pellet was hydrated in 200 μL of nuclease-free water.

Reverse transcription of the RNA was performed using ReverTra Ace qPCR RT Master Mix with gDNA Remover (FSQ-301; Toyobo Co., Ltd., Osaka, Japan) following the manufacturer's protocol. To remove genomic DNA, 0.5 μg of the obtained RNA and DN Master Mix with gDNA Remover were mixed, and the mixture was incubated at 37 °C for 5 min. Two microliters of this mixture was reverse-transcribed using RT Master Mix II containing random primers and oligo dT primers.

qPCR was performed using the SYBR Green qPCR Master Mix (Thermo Fisher Scientific, A66732), according to the manufacturer's protocol. Briefly, the reaction mixture (1× Thermo Scientific SYBR Green qPCR Master Mix, 400 nM forward primer, 400 nM reverse primer, and 2 μL cDNA in nuclease-free water, total volume of 10 μL) was applied to a 384-well PCR plate, and qPCR was performed using LightCycler 480 (Roche). qPCR primers were designed for the EV-D68 MO strain (5′-ACAACATCAAGTATGGTCCC-3′ and 5′-TTGGGA-CACCTTGAGTAATG-3′). The PCR protocol was as follows: (1) pre-incubation step of 2 min at 95 °C, (2) 50 cycles of amplification (95 °C for 5 s, 60 °C for 30 s), and (3) melting curve analysis (95 °C for 15 s, 60 °C for 1 min, and heating to 95 °C at a rate of 0.04 °C/s). LightCycler 480 software (Roche) was used for data acquisition and analysis.

2.19. Statistical analyses

Statistical analyses were performed using Prism 10 software version 10.2.2 (GraphPad Software, San Diego, CA, USA). Significant differences were identified using Tukey's test or Student's *t*-test. Statistical significance was set at $P < 0.05$. The experiment to isolate the MRC-5 and Vero cell-adapted EV-D68 strains was conducted once, and the other experiments were conducted at least three times. Data are representative of one of multiple independent experiments.

3. Results

3.1. Adaptation of EV-D68 to MRC-5 and Vero cells

To develop EV-D68 strains that can replicate in vaccine-manufacturing cells, we first adapted EV-D68 to MRC-5 cells. The adaptation scheme is illustrated in Fig. 1a. We used the US/MO/14–18,947 (MO strain, clade B1), US/KY/14–18,953 (KY strain, clade D), and US/IL/14–18,952 (IL strain, clade B2) strains isolated during the 2014 US outbreak as parental strains. A general strategy for adapting viruses to specific cells involves serial viral passages, in which the virus is inoculated into target cells, the culture is collected, and then inoculated into fresh cells, repeating this process. We attempted to adapt EV-D68 to MRC-5 cells using serial viral passages (Fig. 1a–i). All parental strains initially exhibited limited replication ability in MRC-5 cells (Fig. 1b–d, left panel, black line). After five passages, the strains replicated efficiently, and MRC-5 cell-adapted strains (MO-MRC-passage 5 [P5], KY-MRC-P5, and IL-MRC-P5) were successfully isolated (Fig. 1b–d, left panel, red line). Next, we attempted to adapt EV-D68 to Vero cells using serial viral passages (Fig. 1a–ii). However, none of the strains replicated in Vero cells, even after 15 passages, and we were unable to isolate Vero cell-adapted strains. Next, we attempted to obtain Vero cell-adapted strains by serial passaging of MRC-5 cell-adapted strains in Vero cells (Fig. 1a–iii). All MRC-5 cell-adapted strains replicated in Vero cells, albeit at low levels (Fig. 1b–d, middle panel, red line). After 15 passages in Vero cells, the strains replicated efficiently, and Vero cell-adapted strains (MO-Vero-P15, KY-Vero-P15, and IL-Vero-P15) were successfully isolated (Fig. 1b–d, middle panel, blue line). Table 1 presents the titers of representative viruses in serial passages in MRC-5 and Vero cells. To evaluate the characteristics of the adapted strains, we measured their growth in rhabdomyosarcoma A (RD-A) cells, which are commonly used for EV-D68 culture. All the adapted strains exhibited replication kinetics similar to those of their respective parental strains, indicating that their growth characteristics in RD-A cells were mostly unchanged (Fig. 1b–d, right panel). The maximum viral titers of the MRC-5 and Vero cell-adapted strains were comparable to those of each parental strain in RD-A cells (Fig. 1b–d). In addition, we performed a control experiment involving 20 serial passages of EV-D68 in RD-A cells and evaluated the growth of strains passaged 5 (RD-P5) and 20 times (RD-P20). The MO strain passaged 5 times in RD-A cells (MO-RD-P5) grew in MRC-5 cells and the IL strain passaged 20 times in RD-A cells (IL-RD-P20) grew in Vero cells (Supplementary Fig. 1a–f). However, none of the RD-A cell-passaged strains grew more efficiently than the MRC-5 and Vero cell-adapted strains (Supplementary Fig. 1a–f). Thus, we found that specific adaptation to MRC-5 and Vero cells, rather than adaptation to general cells, was important for efficient replication. These results indicate that the method of adaptation to Vero cells via adaptation to MRC-5 cells can be applied to EV-D68 strains belonging to various clades.

3.2. Characterization of MRC-5 and Vero cell-adapted EV-D68 strains

To characterize the populations of the adapted strains, five viral clones were isolated from each Vero cell-adapted strain using plaque isolation. Evaluation of the replication kinetics of each viral clone in Vero cells revealed no substantial differences in replication efficiency, except for the slow growth of KY-Vero-P15-#3 (Fig. 2a–c). We then analyzed the sequences of the isolated strains to identify mutations acquired during the adaptation process (Fig. 2d, Tables 2–4). Sequence analysis of bulk viruses detected several mutations in both the MRC-5

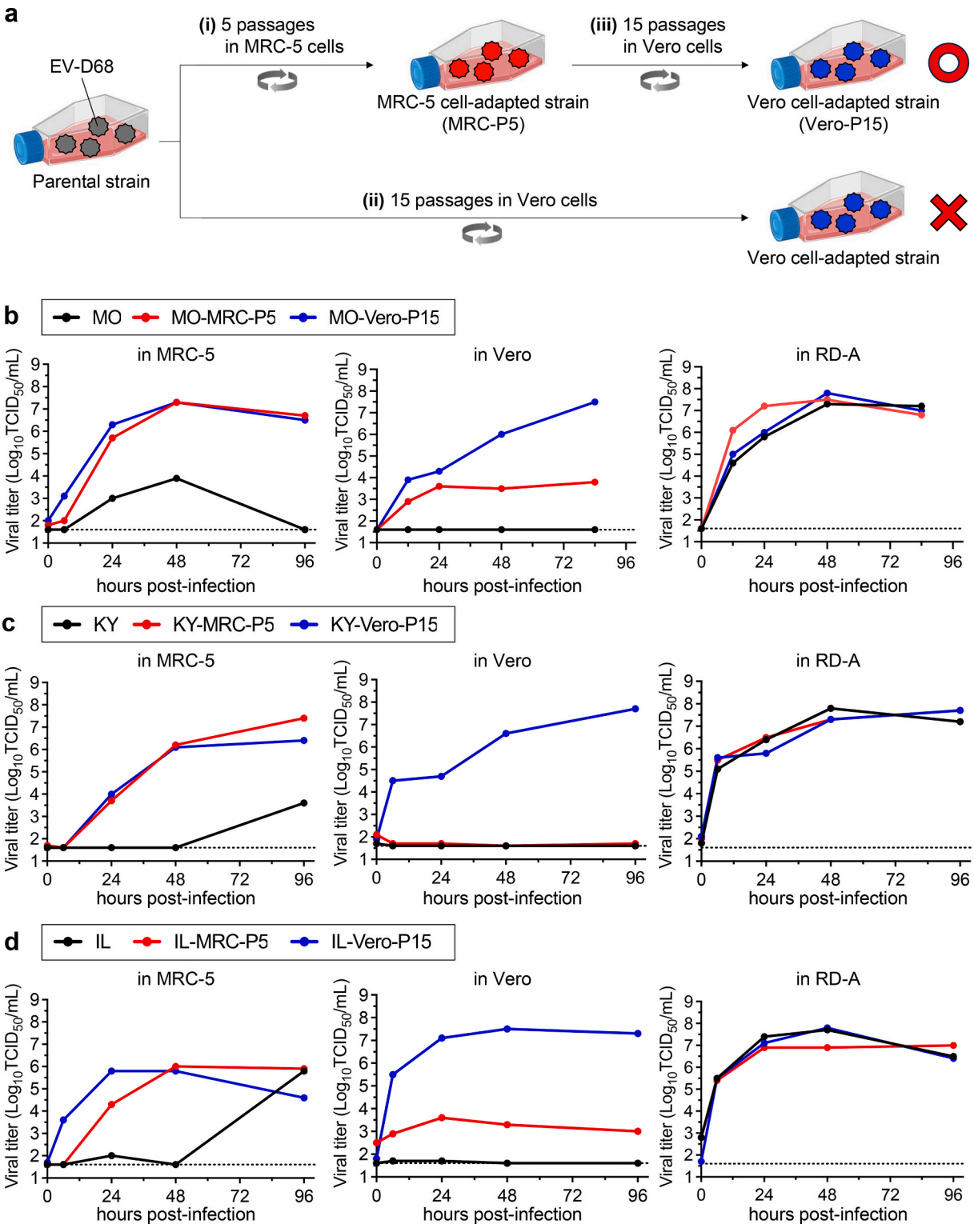

Fig. 1. Adaptation of EV-D68 to MRC-5 and Vero cells. (a) Adaptation scheme. (i) EV-D68 was adapted to MRC-5 cells through five passages in MRC-5 cells. (ii) EV-D68 was not adapted to Vero cells after 15 passages in Vero cells. (iii) The MRC-5 cell-adapted strain was adapted to Vero cells through 15 passages in Vero cells. The image was created using BioRender.com. (b–d) The time course of viral titers was evaluated after infecting MRC-5, Vero, or RD-A cells with each parental, MRC-5 cell-adapted, and Vero cell-adapted strain. The left panel shows the time course of the viral titer in MRC-5 cells, the middle panel in Vero cells, and the right panel in RD-A cells. Dotted lines indicate the limits of detection.

and Vero cell-adapted strains, including mutations involving amino acid substitutions in the structural and non-structural protein regions (Fig. 2d, Tables 2–4). VP3-E59D, VP3-A126T, VP1-N27H, VP1-D87N, and VP1-D285G were detected in MO-MRC-P5 (Fig. 2d, Table 2); VP1-F74I, VP1-E83G, VP1-M135K, and 3D-H348Q were detected in KY-MRC-P5 (Fig. 2d, Table 3); and VP3-D237N and VP1-E271G were detected in IL-MRC-P5 (Fig. 2d, Table 4). There was no concordance in the location of the mutations and amino acid changes among MO-MRC-

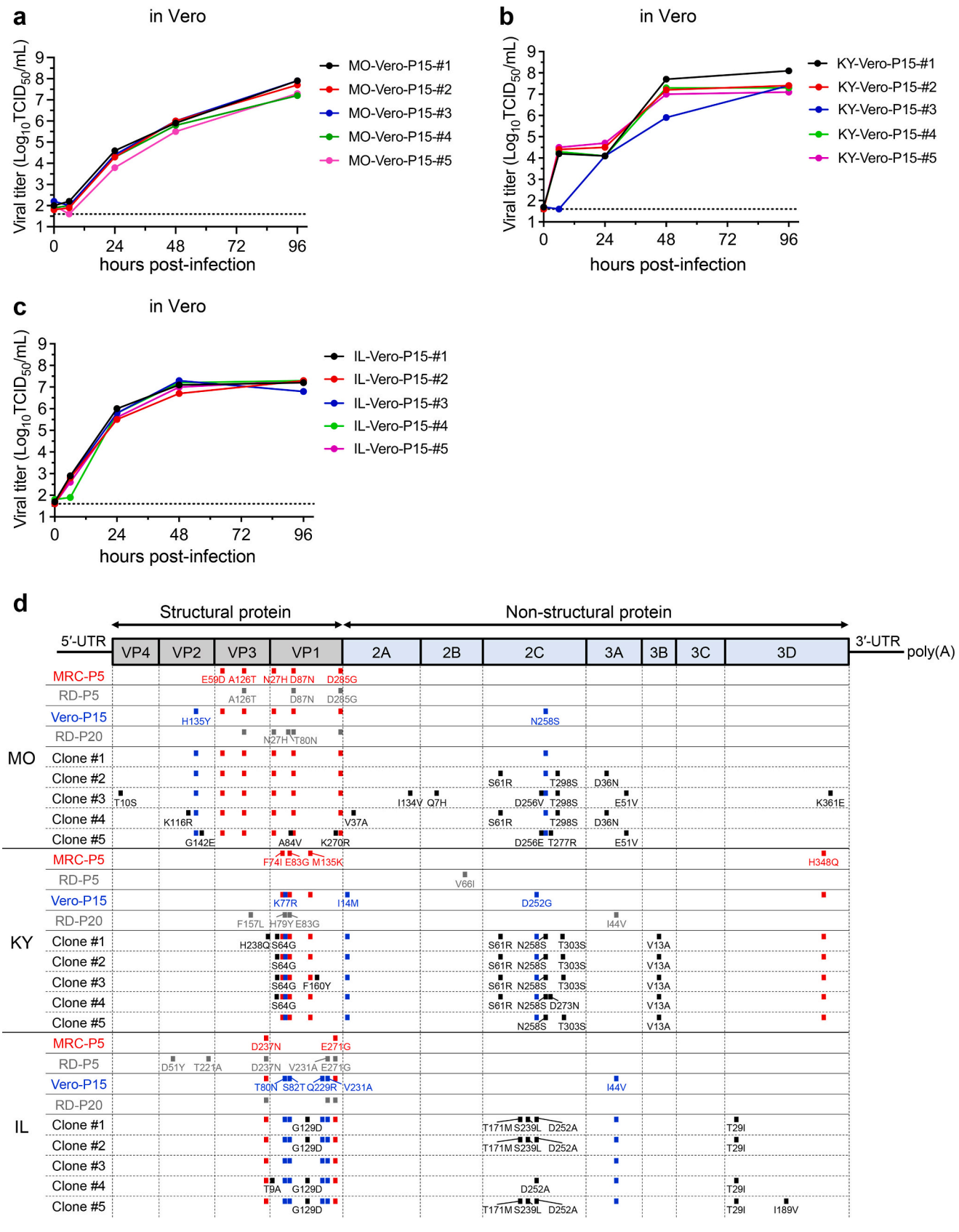

Fig. 2. Characterization of MRC-5 and Vero cell-adapted strains. (a–c) Growth curves of viral clones isolated from Vero cell-adapted strains. The time course of viral titers was evaluated after infecting Vero cells with viral clones isolated from Vero cell-adapted (a) MO, (b) KY, and (c) IL strains at an MOI of 0.1. (d) Sequence analysis of RD-A cell-passaged strains, MRC-5 cell-adapted strains, Vero cell-adapted strains, and clones isolated from Vero cell-adapted strains. The amino acid mutations detected in structural and non-structural proteins were mapped to the EV-D68 genome.

Table 2
Amino acid substitutions in each cell-adapted strain derived from the MO strain.

Protein	Position	Neutralizing antigenic site	Wild type MO	RD-P5	RD-P20	MRC-P5	Vero-P15	Vero-P15 Clones				
								#1	#2	#3	#4	#5
VP4	10[a]	–	T[b] (act)[c]				–			S (tct)	–	–
	116		K (aaa)			–				–	R (aga)	
VP2	135	Near Site II	H (cac)	–			Y (tac)					
	142	–	G (ggg)				–					E (gag)
VP3	59	Near Site III	E (gaa)			D (gat)						
	126		A (gcg)	T (acg)								
VP1	27	–	N (aat)		H (cat)							
	80		T (act)	–	N (aat)		–					
	84		A (gca)		–							V (gta)
	87	Site I	D (gac)	N (aac)								
	270	–	K (aaa)	–								R (aga)
	285	Site III	D (gac)	G (ggc)								
2A	37		V (gtc)							–	A (gcc)	
	134		I (atc)						–	V (gtc)	–	
2B	7		Q (caa)							H (cac)		–
	61		S (agt)				–		R (aga)	–	R (aga)	
2C	256		D (gac)						–	V (gtc)	–	
	258		N (aat)	–			S (agt)			–		E (gaa)
	277		T (acg)						–			R (agg)
	298		T (act)						S (tct)			
3A	36		D (gat)				–		N (aat)	–	N (aat)	–
	51		E (gag)							V (gtg)		V (gtg)
3D	361		K (aaa)						–	E (gaa)	–	–

[a] Amino acid positions are numbered with the N-terminal amino acid of each structural and non-structural protein as 1.
[b] Amino acid.
[c] Codon.

Table 3
Amino acid substitutions in each cell-adapted strain derived from the KY strain.

Protein	Position	Neutralizing antigenic site	Wild type KY	RD-P5	RD-P20	MRC-P5	Vero-P15	Vero-P15 Clones				
								#1	#2	#3	#4	#5
VP3	157[a]		F[b] (ttt)[c]	–	L (ctt)	–						
	238	–	H (cat)					Q (cag)	–			–
	64		S (agc)	–		–		G (ggc)				
	74		F (ttc)			I (atc)						
VP1	77	Near Site I	K (aaa)			–	R (aga)					
	79		H (cac)		Y (tac)	–						
	83		E (gaa)	–	G (gga)							
	135	–	M (atg)			K (aag)						
	160		F (ttc)	–			–			Y (tac)	–	
2A	14		I (ata)				M (atg)					
2B	66		V (gtc)	I (atc)	–		–					
	61		S (agc)				–	R (agg)				–
	252		D (gat)				G (ggt)					
2C	258		N (aat)	–		–		S (agt)				
	273		D (gac)					–			N (aac)	–
	303		T (act)				–	S (tct)			–	S (tct)
3A	44		I (att)	–	V (gtt)			–				
3B	13		V (gta)	–				A (gca)				
3D	348		H (cat)			Q (cag)						

[a] Amino acid positions are numbered with the N-terminal amino acid of each structural and non-structural protein as 1.
[b] Amino acid.
[c] Codon.

P5, KY-MRC-P5, and IL-MRC-P5. Sequence analysis of the Vero cell-adapted strains revealed the following additional mutations: VP2-H135Y and 2C-N258S in MO-Vero-P15 (Fig. 2d, Table 2); VP1-K77R, 2 A-I14M, and 2C-D252G in KY-Vero-P15 (Fig. 2d, Table 3); and VP1-T80N, VP1-S82T, VP1-Q229R, VP1-V231A, and 3 A-I44V in IL-Vero-P15 (Fig. 2d, Table 4). Similar to the MRC-5 cell-adapted strains, the location of mutations and amino acid changes were not consistent among MO-Vero-P15, KY-Vero-P15, and IL-Vero-P15. In addition, sequence analysis of clones isolated from Vero cell-adapted strains revealed additional mutations in some clones that were not detected in bulk viruses (Fig. 2d, Tables 2–4). All mutations detected in the bulk viruses were also detected in all clones isolated from Vero cell-adapted strains derived from any parental strain (Tables 2–4). For the clones MO-Vero-P15-#1 and IL-Vero-P15-#3, only mutations detected in bulk viruses were detected (Tables 2–4). Furthermore, mutations detected in the control RD-A cell-passaged strains were partially shared by mutations detected in MRC-5 and Vero cell-adapted strains (Fig. 2d, Tables 2–5). Thus, we found that there are mutations acquired by general cell passaging and those acquired by specific passaging in MRC-5 and Vero cells.

The cell surface receptors for EV-D68 have not been fully identified; however, sialic acid and heparan sulfate glycosaminoglycans have been

Table 4
Amino acid substitutions in each cell-adapted strain derived from the IL strain.

Protein	Position	Neutralizing antigenic site	Wild type IL	RD-P5	RD-P20	MRC-P5	Vero-P15	Vero-P15 Clones				
								#1	#2	#3	#4	#5
VP2	51[a]	–	D[b] (gat)[c]	Y (tat)	–							
	221		T (aca)	A (gca)								
VP3	237		D (gac)	N (aac)								
	9	Near Site I	T (act)				–				A (gct)	–
	80		T (act)				N (aat)					
	82		S (tct)	–		–	T (act)					
VP1	129		G (ggt)				–	D (gat)		–	D (gat)	
	229	–	Q (caa)				R (cga)					
	231		V (gtt)	A (gct)			A (gct)					
	271		E (gag)	G (ggg)								
	171		T (acg)					M (atg)			–	M (atg)
2C	239		S (tca)				–	L (tta)		–		L (tta)
	252		D (gac)	–				A (gcc)			A (gcc)	
3A	44		I (att)				V (gtt)					
3D	29		T (aca)				–	I (ata)			I (ata)	
	189		I (att)					–		–	–	V (gtt)

[a] Amino acid positions are numbered with the N-terminal amino acid of each structural and non-structural protein as 1.
[b] Amino acid.
[c] Codon.

Table 5
Amino acid substitutions in each RD-A cell-passaged strain.

	Protein	Position	Wild type	RD-P5	RD-P20
MO	VP3	126[a]	A[b] (gcg)[c]	T (acg)	
	VP1	27	N (aat)	–	H (cat)
		80	T (act)		N (aat)
		87	D (gac)	N (aac)	
		285	D (gac)	G (ggc)	
KY	VP3	157	F (ttt)		L (ctt)
	VP1	79	H (cac)	–	Y (tac)
		83	E (gaa)		G (gga)
	2B	66	V (gtc)	I (atc)	–
	3A	44	I (att)	–	V (gtt)
IL	VP2	51	D (gat)	Y (tat)	–
		221	T (aca)	A (gca)	
	VP3	237	D (gac)	N (aac)	
	VP1	231	V (gtt)	A (gct)	
		271	E (gag)	G (ggg)	

[a] Amino acid positions are numbered with the N-terminal amino acid of each structural protein as 1.
[b] Amino acid.
[c] Codon.

reported as receptors for EV-D68 [32,34–36]. Therefore, we examined the dependence of the parental and Vero cell-adapted strains on sialic acid and heparan sulfate glycosaminoglycans during infection. *N*-acetylneuraminic acid was used as a sialic acid analog, and heparin was used as a heparan sulfate glycosaminoglycan analog [36–38]. Replication of all parental strains in RD-A cells and Vero cell-adapted strains in Vero cells was not inhibited in the presence of 0.04–5 mg/mL sialic acid (Fig. 3a–f, blue line). However, in the presence of 25 mg/mL sialic acid, replication was inhibited to a level at which the virus could not be detected (Fig. 3a–f, blue line). Replication of IL-Vero-P15 was slightly inhibited in the presence of 5–25 mg/mL heparin, but replication of other strains was hardly inhibited by heparin at any concentration (Fig. 3a–f, red line). These results indicate that sialic acid is particularly important for infection by both strains, whereas heparan sulfate glycosaminoglycan is not essential.

3.3. Preparation and characterization of the inactivated WV vaccines

Inactivated WV vaccines were prepared to evaluate the immunogenicity of isolated MRC-5 and Vero cell-adapted strains. The parental MO strain was propagated in RD-A cells, the MRC-5 cell-adapted strain in MRC-5 cells, and the Vero cell-adapted strains in Vero cells. For the Vero cell-adapted strains, MO-Vero-P15-#1 and MO-Vero-P15-#5 were selected as representative clones, based on the lowest and highest number of mutations detected, respectively. After inactivation of EV-D68 with β-propiolactone, full particles containing the viral RNA genome were obtained by sucrose density gradient ultracentrifugation, as previously reported [18]. SDS-PAGE revealed that the bands corresponding to VP1, VP2, and VP3 were detected for all inactivated WV vaccines (Fig. 4a). In lane 1, corresponding to the parental MO strain, a protein band was detected at around 10 kDa, but no such band was observed in the other lanes, corresponding to each adapted strain (Fig. 4a). In addition, the size of VP1 appeared to be smaller in each adapted strain compared to the parental MO strain (Fig. 4a). Dynamic light scattering analysis revealed the presence of structures of approximately 30 nm in size, which appeared to be EV-D68 particles (Fig. 4b). In addition, spherical particles with a diameter of approximately 30 nm were detected by negative-stain TEM of the inactivated WV vaccines prepared from the parental MO and MO-Vero-P15 strains (Fig. 4c). Inactivated WV vaccines derived from KY, KY-Vero-P15, IL, and IL-Vero-P15 were prepared using the same method. The SDS-PAGE data are shown in Supplementary Fig. 2. Therefore, we prepared inactivated WV vaccines derived from the MRC-5 and Vero cell-adapted strains.

3.4. Vaccine effect of inactivated WVs prepared from MRC-5 and Vero cell-adapted MO (clade B1) strains in mice

We previously reported that an inactivated WV vaccine prepared from the MO strain induces potent antibody responses and protective effects in mice [18]. To evaluate the ability of the inactivated WV vaccines prepared from MO-MRC-P5, MO-Vero-P15, MO-Vero-P15-#1, and MO-Vero-P15-#5 to induce antibody responses and protective effects, mice were subcutaneously immunized with inactivated WV on days 0 and 21. Antibody production was evaluated by ELISA, using the live parental MO strain as the coating antigen. MO-specific IgG antibody levels after prime (day 14) and boost (day 28) immunizations were significantly higher in all immunized groups than those in the PBS-treated group (Fig. 5a). MO-specific IgG antibody levels were comparable in all immunized groups. Next, we evaluated neutralizing antibody titers against the parental MO strain. Consistent with the antibody production levels, neutralizing antibody titers against the parental MO strain after boost immunization were significantly higher in all immunized groups than in the PBS-treated group, and were comparable in all immunized groups (Fig. 5b). Next, we evaluated the protective effects of

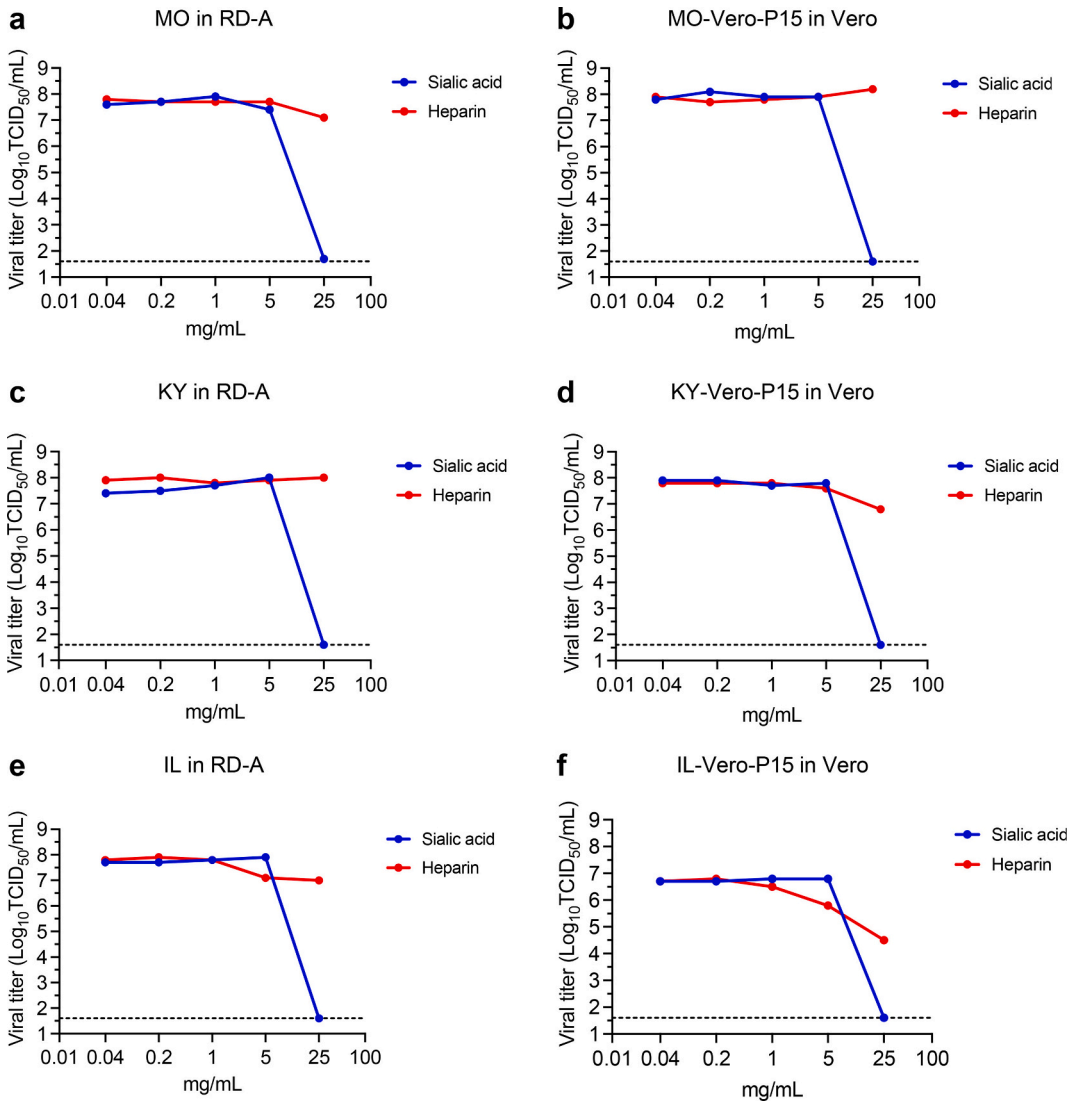

Fig. 3. Dependence on sialic acid and heparin in EV-D68 infection. (a–f) Evaluation of EV-D68-infection dependence on sialic acid and heparin. RD-A cells were infected with the parental (a) MO, (c) KY, or (e) IL strains in the presence of 0.04–25 mg/mL sialic acid or heparin. Vero cells were infected with the (b) MO-Vero-P15, (d) KY-Vero-P15, or (f) IL-Vero-P15 strains in the presence of 0.04–25 mg/mL sialic acid or heparin. Viral titers were evaluated 3 days post-infection. Dotted lines indicate the limits of detection.

inactivated WV vaccines against EV-D68 challenge. Immunized mice were intranasally challenged with the MO strain at 5×10^6 $TCID_{50}$. In this infection model, an increase in viral titers (Supplementary Fig. 3a) and total EV-D68 RNA copy numbers (Supplementary Fig. 3b) in the lungs was observed between 4 and 12 h post-infection. This observation is consistent with that of a previous study using the same infection model as ours [39]. Therefore, viral loads in the nasal turbinates and lungs were measured 12 h after challenge and were significantly reduced in all immunized groups compared to those in the PBS-treated group (Fig. 5c). The protective effect was comparable in all the immunized groups. Thus, similar to the inactivated WV vaccine prepared from the parental MO strain, the inactivated WV vaccines prepared from the MRC-5 and Vero cell-adapted MO strains induced protective immunity against EV-D68 infection.

3.5. Vaccine effect of inactivated WVs prepared from Vero cell-adapted KY (clade D) and Vero cell-adapted IL (clade B2) strains in mice

Next, we evaluated the ability of inactivated WV vaccines prepared from Vero cell-adapted KY strains to induce antibody responses and protective effects. Mice were subcutaneously immunized with inactivated WVs prepared from the parental KY and KY-Vero-P15 strains. After prime and boost immunizations, KY-specific IgG antibody levels were significantly higher in both immunized groups than in the PBS-treated group (Fig. 6a). KY-specific IgG antibody levels were comparable between the parental KY and KY-Vero-P15 groups (Fig. 6a). Consistent with the antibody production levels, neutralizing antibody titers against the parental KY strain after boost immunization were significantly higher in both immunized groups than in the PBS-treated group and were comparable in both immunized groups (Fig. 6b). After challenge, the viral loads in the nasal turbinates and lungs were significantly reduced in both immunized groups compared to those in the PBS-treated group (Fig. 6c). Although the neutralizing antibody titers of the parental KY and KY-Vero-P15 groups were comparable (Fig. 6b), the protective effect of the KY-Vero-P15 group was slightly, but significantly, lower than that of the parental KY group (Fig. 6c). Therefore, although the Vero cell-adapted KY strain was slightly inferior to the parental KY strain, it was sufficiently immunogenic to induce neutralizing antibodies and protect against EV-D68 infection.

Next, mice were subcutaneously immunized with inactivated WVs prepared from the parental IL and IL-Vero-P15 strains. After prime and boost immunizations, IL-specific IgG antibody levels were significantly

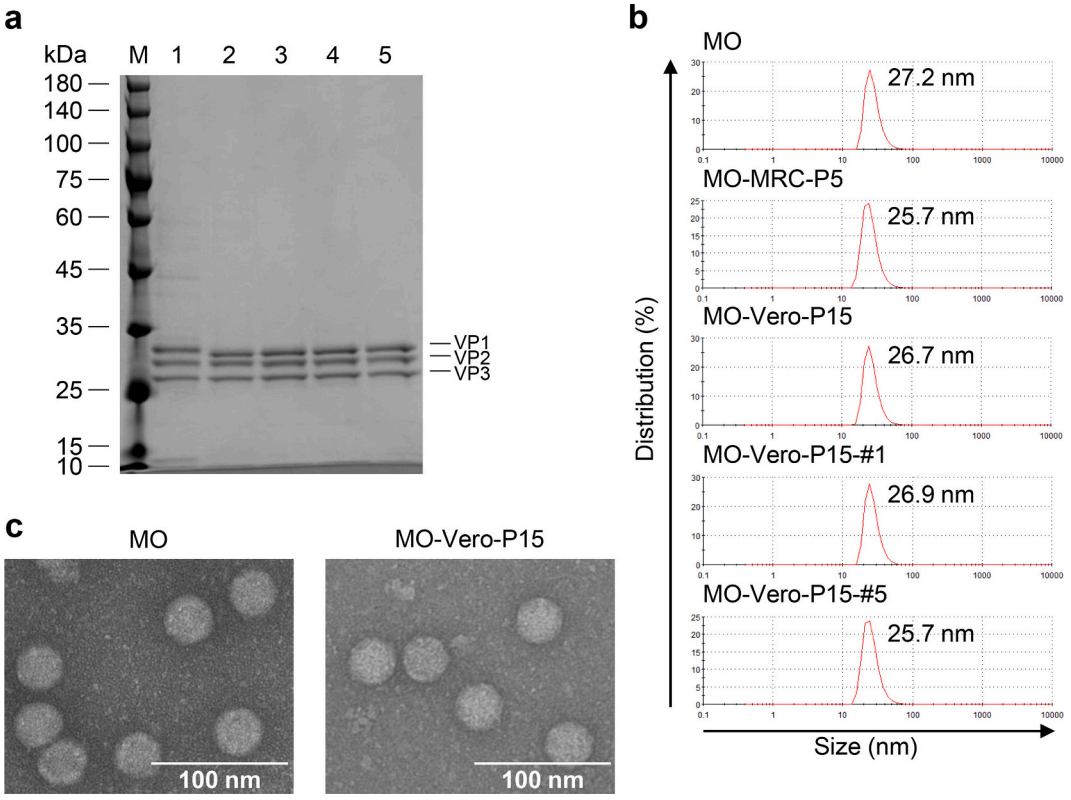

Fig. 4. Properties of inactivated WVs prepared from MRC-5 and Vero cell-adapted MO strains. (a) SDS-PAGE analysis. M: protein marker. Lane 1: MO, Lane 2: MO-MRC-P5, Lane 3: MO-Vero-P15, Lane 4: MO-Vero-P15-#1, Lane 5: MO-Vero-P15-#5. (b) Dynamic light scattering measurements of the inactivated WVs. (c) Representative TEM images of the inactivated WVs prepared from the MO and MO-Vero-P15 strains. Scale bars = 100 nm.

higher in both immunized groups than in the PBS-treated group (Fig. 6d). IL-specific IgG antibody levels were comparable between the parental IL and IL-Vero-P15 groups (Fig. 6d). Neutralizing antibody titers against the parental IL strain after boost immunization in the parental IL strain group were significantly higher than those in the PBS-treated group (Fig. 6e). However, neutralizing antibody titers were barely detectable in the IL-Vero-P15 group (Fig. 6e). The parental IL strain group showed significantly higher neutralizing antibody titers against IL-Vero-P15 than the PBS-treated group; however, the titer appeared to be lower than that against the parental IL strain (Supplementary Fig. 4). Consistent with the neutralizing antibody titer data, viral loads in the nasal turbinates and lungs were significantly reduced in the parental IL strain group compared to those in the PBS-treated group (Fig. 6f). In contrast, the IL-Vero-P15 group showed almost no protective effect (Fig. 6f). These data indicate that in some cases, immunogenicity is substantially reduced through adaptation.

4. Discussion

In a previous study, a Vero cell-adapted KY strain was isolated by the serial passage of EV-D68 in Vero cells [17]. However, we were unable to adapt any EV-D68 strain used in this study, including the KY strain, to Vero cells by serial viral passages in Vero cells. This difference may be due to the origin and maintenance conditions of the Vero cells, and the method of preparation of the parental viral stock. In addition, it may be due to low input viral titer in direct passages in Vero cells. In the previous study, mutations VP3-V24L, VP1-E83G, VP1-M135K, VP1-E155K, 2C-D247N, 2C-T298S, and 3D-H348Q were identified [17]. The mutations VP1-E83G, VP1-M135K, and 3D-H348Q reported in the previous study [17] were also detected in the Vero cell-adapted KY strain isolated in the current study. Therefore, these common mutations may be particularly important for the adaptation of the KY strain.

In this study, it was unclear why EV-D68 came to be able to replicate in MRC-5 and Vero cells. Sialic acid, heparan sulfate glycosaminoglycans, and intercellular adhesion molecule 5 (ICAM-5) are putative EV-D68 receptors [32,34–36]. Sialic acid and heparan sulfate glycosaminoglycans have been reported to be expressed in RD and Vero cells [34,40–42]. ICAM-5 has also been reported to be expressed in RD cells but not in Vero cells [32]. Therefore, we investigated the dependence on sialic acid and heparan sulfate glycosaminoglycans during infection. We found that both the parental and Vero cell-adapted strains shared the characteristic of using sialic acid rather than heparan sulfate glycosaminoglycans for cellular infection. We found no difference in dependence on these molecules; however, there may be other receptors for EV-D68 [35,43–46]. In addition, major facilitator superfamily domain containing 6 (MFSD6) was recently identified as an entry receptor for EV-D68 [47,48]. Cryo-electron microscopy (cryo-EM) revealed that the EV-D68 IL strain interacts with MFSD6 via specific residues in VP1 (K92, T94, G151, L208, T216, N219, I262), VP2 (T137, T139, S140), and VP3 (A245, Q247) [48]. These amino acid residues remained unchanged following the adaptation of all strains used to adapt to MRC-5 cells and Vero cells, indicating that the adaptation process likely does not alter the interaction between EV-D68 and MFSD6. Furthermore, we demonstrated, through control passage experiments using RD-A cells, the occurrence of both adaptive mutations to general cells and adaptive mutations specific to MRC-5 cells and Vero cells. Most of the capsid mutations acquired by general cell passaging were accompanied by amino acid changes toward positive charges. These capsid mutations, accompanied by positive charge changes, may have enhanced the interaction between EV-D68 and the host cell membrane.

Mutations in non-structural proteins may also affect the ability of EV-D68 to replicate in MRC-5 and Vero cells. Among the non-structural proteins, mutations were detected in the 2 A, 2B, 2C, 3 A, 3B, and 3D proteins. Enteroviral 2 A has been reported to function as a protease, 2B

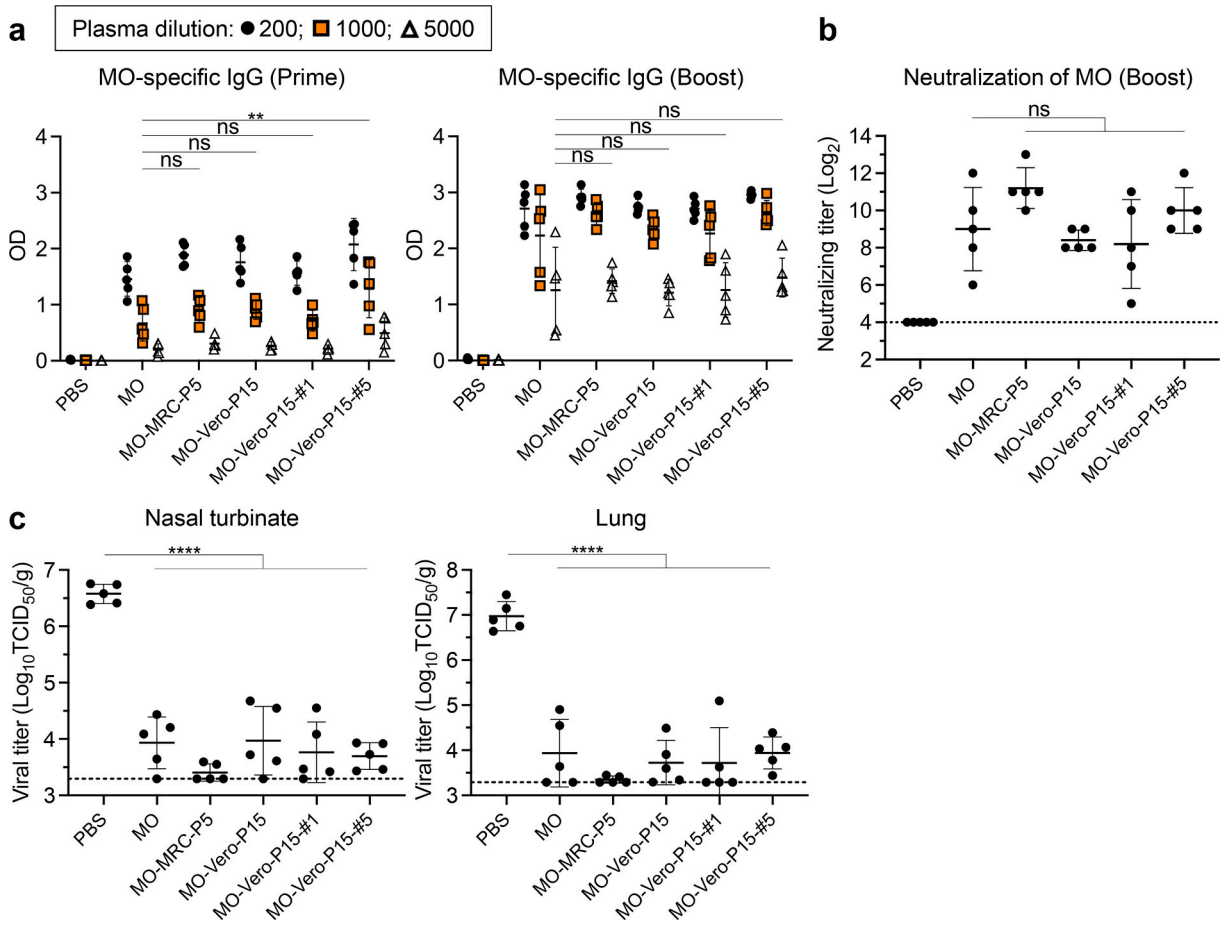

Fig. 5. Vaccine effect of inactivated WVs prepared from MRC-5 and Vero cell-adapted MO strains. Mice were subcutaneously immunized twice with inactivated WV vaccines. (a) Parental MO strain-specific IgG antibody levels in the plasma after prime (left panel) and boost (right panel) immunization. (b) Neutralizing antibody titers against the parental MO strain determined after boost immunization. (c) Mice were intranasally challenged with the parental MO strain after boost immunization. Viral loads in nasal turbinates (left panel) and lungs (right panel) were measured 12 h after challenge. (a–c) $n = 5$ per group. Data are shown as the mean ± SD. (b, c) Dotted lines indicate the limits of detection. (a) Significant differences were analyzed in 1000- or 5000-fold-diluted plasma samples. (a–c) "ns" indicates not significant. **, $P < 0.01$; ****, $P < 0.0001$ as indicated by Tukey's test.

as a viroporin, 2C as a helicase and RNA chaperone, 3 A as a component of replication organelles, 3B as a primer for RNA replication, and 3D as an RNA-dependent RNA polymerase [2,49,50]. Therefore, the 2 A mutation may have facilitated an increase in the proteolytic cleavage efficiency of the precursor polypeptide, the 2B mutation may have enhanced the efficiency of virion release from the host cell, and the 2C, 3 A, 3B, and 3D mutations may have contributed to the increased RNA replication and translation efficiency. No mutations were detected in the non-structural proteins of the MO and IL strains upon adaptation to MRC-5 cells. In contrast, mutations in non-structural proteins were acquired during adaptation to Vero cells. Thus, in the MO and IL strains, mutations in non-structural proteins appear to be important for adaptation to Vero cells. In the KY strain, mutations in non-structural proteins were acquired during the adaptation to both MRC-5 and Vero cells. Therefore, in the KY strain, mutations in non-structural proteins appear to be important for adaptation to both MRC-5 and Vero cells. Furthermore, no mutations were detected in non-structural proteins in MO and IL strains passaged 20 times in RD-A cells. Mutations detected in non-structural proteins in KY strains passaged 20 times in RD-A cells did not match those acquired in the Vero cell-adapted KY strain. These results suggest that adaptation of non-structural proteins is important for the gain of tropism for Vero cells.

Although mutations acquired through adaptation may be important for efficient replication in each cell, they may also alter immunogenicity. The adaptation of EV-D68 and other enteroviruses to Vero and MRC-5 cells has also been reported in several studies; however, whether immunogenicity is altered during the adaptation process has not been evaluated [17,51–55]. For the MO and KY strains, immunogenicity remained largely unchanged, although there was a slight yet significant decrease in the protective efficacy against EV-D68 infection in the KY strain. However, in the IL strain, although the level of antibody production was comparable to that of the parental strain, the ability to induce neutralizing antibodies and the protective effect were impaired to levels similar to those in the PBS-treated group. Recently, four neutralizing antigenic sites, defined as clusters of neutralizing antibody epitopes, were identified on the EV-D68 capsid [56]. Mutations detected in the vaccine-manufacturing cell-adapted strains at or near these sites may affect their ability to induce neutralizing antibodies. Based on the cryo-EM structure of EV-D68, we sought to understand the relationship between the mutant residues identified in the Vero cell-adapted strains and the neutralizing antigenic sites. Although the cryo-EM structure of the MO strain has been reported [57], the structures of the KY and IL strains remain unreported. Therefore, all strains were analyzed based on the cryo-EM structure of the MO strain (PDB ID: 6CSG) [57]. Among the residues exhibiting mutations in the Vero cell-adapted MO strain, VP1-D87 is located at site I, VP2-H135 near site II, and VP1-D285 and VP3-E59 at or near site III (Table 2). In the Vero cell-adapted KY strain, VP1-F74, VP1-K77, and VP1-E83 are located near site I (Table 3). In the Vero cell-adapted IL strain, VP1-T80 and VP1-S82 are located near site I (Table 4). Thus, mutations near the neutralizing antigenic sites were

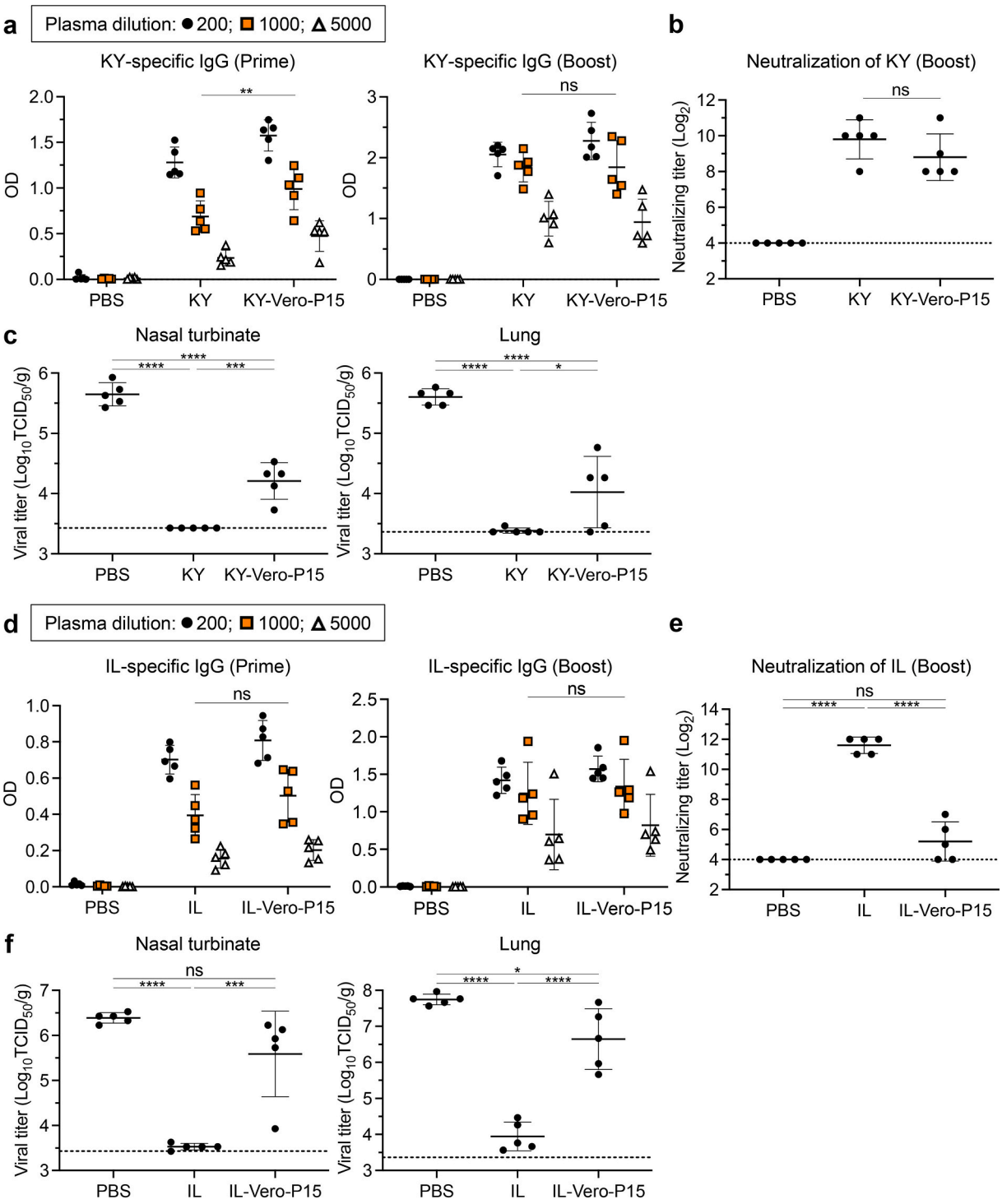

Fig. 6. Vaccine effect of inactivated WVs prepared from Vero cell-adapted KY and IL strains. Mice were subcutaneously immunized twice with inactivated WV vaccines prepared from KY-Vero-P15 (a–c) or IL-Vero-P15 (d–f). (a, d) Parental KY (a) or IL (d) strain-specific IgG antibody levels in plasma after prime (left panel) and boost (right panel) immunization. (b, e) Neutralizing antibody titers against the parental KY (b) or IL (e) strain determined after boost immunization. (c, f) Mice were intranasally challenged with the parental KY (c) or IL (f) strain after boost immunization. Viral loads in nasal turbinates (left panel) and lungs (right panel) were measured 12 h after challenge. (a–f) $n = 5$ per group. Data are shown as the mean ± SD. (b, c, e, f) Dotted lines indicate the limits of detection. (a, d) Significant differences were analyzed in 1000-fold-diluted plasma samples. (a–f) "ns" indicates not significant. *, $P < 0.05$; **, $P < 0.01$; ***, $P < 0.001$; ****, $P < 0.0001$ as indicated by Tukey's test.

dispersed among the three neutralizing antigenic sites (I, II, and III) in the MO strain but were concentrated at site I in the KY and IL strains. In the Vero cell-adapted MO strain, the distribution of mutations at multiple neutralizing antigenic sites may help avoid a decrease in immunogenicity. The Vero cell-adapted KY and IL strains were similar in that the mutations were concentrated near site I. In addition, as described above, since none of the adapted strains harbor mutations in the regions essential for interaction with MFSD6, it is presumed that antibodies targeting these regions are being induced. However, the immunogenicity of the Vero cell-adapted IL strain was considerably low. The cause

of this difference is unclear, but it is possible that a mutation in the IL strain had a substantial effect on the conformation of the neutralizing antigen sites, reducing its ability to induce neutralizing antibodies. However, the cryo-EM structure and neutralizing antigenic sites of KY and IL strains have not been identified; therefore, further detailed analysis is important. If the mutations responsible for adaptation can be identified, and adaptation can be achieved with minimal mutations, a reduction in immunogenicity may be avoided. In addition, the finding that there is a risk of altered immunogenicity through adaptation to target cells indicates that it is important to screen for viral strains with unaltered immunogenicity, such as MO strains. Although we only evaluated the immunogenicity of clones derived from Vero cell-adapted MO strain, further studies on the immunogenicity of clones derived from Vero cell-adapted KY and IL strains are also important.

In a previous study [18], where we used the same EV-D68 mouse infection model as that used in this study, we found that subcutaneous immunization of mice with an inactivated WV vaccine prepared from the MO strain led to the detection of EV-D68-specific IgG antibodies, but not EV-D68-specific IgA antibodies, in the nasal wash and lungs, and EV-D68-specific IgG antibodies may have contributed to the protective effect. Therefore, in this study, EV-D68-specific IgG antibodies were considered to play an important role in the protective effect. As no symptoms of EV-D68 infection were observed in this mouse model, it was not possible to evaluate the protective effect of the vaccine against symptoms. On the contrary, we evaluated the neutralizing antibody titer against EV-D68 because it is generally regarded as an important indicator that correlates with protection by vaccines against many picornaviruses [58,59].

SDS-PAGE analysis of the inactivated WV vaccines revealed a band at around 10 kDa in the parental MO strain, which was not detected in any of the cell-adapted strains. This band may correspond to VP4, based on its molecular weight. However, we could not investigate this because antibodies against VP4 were not available. If this band is VP4, A-particles lacking VP4 might have been generated in each adapted strain due to instability. Meanwhile, these adapted strains exhibited immunogenicity comparable to that of the parental MO strain. Furthermore, the size of VP1 appeared to be smaller in each adapted strain compared to the parental MO strain. It is unclear whether the size shift is related to amino acid changes or proteolytic differences. Therefore, further detailed antigenic property analysis is necessary.

Several aspects of the present study remain unexamined. Notably, the safety profile of the vaccine was not evaluated, which is a major concern. Common side effects of inactivated WV vaccines, such as fever, inflammation, and pain at the injection site [60–62], may also be associated with our vaccine. However, further research on the safety of the vaccine is required. During the production of inactivated WV vaccines, there is a risk of infection for the vaccine manufacturer and potential for accidental viral release. Therefore, further research is required to investigate the virulence of the vaccine-manufacturing cell-adapted EV-D68 strains. Additionally, if the virus acquires further mutations during the culture process of vaccine manufacturing, its immunogenicity may change. Therefore, further studies are required to evaluate the genetic stability of each cell-adapted strain. Furthermore, only three strains belonging to clades B1, B2, and D, isolated during the 2014 outbreak in the US, were used in this study. Thus, it is important to investigate the applicability of our adaptation methods to a broader range of EV-D68 strains, particularly those belonging to clade B3, which have been frequently detected [63–66]. It is also important to investigate whether our adaptation method can be applied to viruses other than EV-D68.

In conclusion, we demonstrated that MRC-5 and Vero cell-adapted strains can be efficiently obtained using our original method, which may be applicable to various EV-D68 strains. We also showed that there is a risk of decreased immunogenicity through adaptation in some cases. These findings offer valuable insights for the production of inactivated WV vaccines against EV-D68.

Author contribution

K.S. and Y.Y. designed the experiments. K.S., Y.K., and K.T. performed the experiments. K.S., Y. K., K.T., T.I., and Y.Y. performed the data analysis and interpretation. C.N., Y.K., T.I., T.H., and T.N. designed the experiments and edited the manuscript. K.S. and Y.Y. wrote the manuscript. Y.Y. oversaw the study. All the authors have read and agreed to the published version of this manuscript.

CRediT authorship contribution statement

Kota Senpuku: Writing – review & editing, Writing – original draft, Visualization, Investigation, Funding acquisition, Formal analysis, Data curation, Conceptualization. **Yuta Kunishima:** Methodology, Investigation, Formal analysis, Data curation. **Kotaro Taniguchi:** Investigation, Formal analysis, Data curation. **Taiki Ito:** Writing – review & editing. **Toshiro Hirai:** Writing – review & editing, Investigation. **Teruya Nakamura:** Writing – review & editing, Visualization, Methodology, Formal analysis, Data curation. **Chikako Kataoka-Nakamura:** Writing – review & editing, Investigation. **Yasuo Yoshioka:** Writing – review & editing, Writing – original draft, Supervision, Resources, Project administration, Funding acquisition, Conceptualization.

Funding

This study was supported by grants from the Japan Society for the Promotion of Science (JSPS KAKENHI Grant Number: JP23K27343 and JP24K22020 to Y.Y.), Japan Agency for Medical Research and Development (AMED Grant Number: JP223fa627002 to Y.Y.), the All-Osaka U Research in “The Nippon Foundation-Osaka University Project for Infectious Disease Project” (to Y.Y.), the Japan Science and Technology Agency (JST SPRING Grant Number: JPMJSP2138 to K.S.), and The Research Foundation for Microbial Diseases of Osaka University (BIKEN).

Declaration of competing interest

The authors declare the following financial interests/personal relationships which may be considered as potential competing interests: Yasuo Yoshioka reports financial support was provided by The Research Foundation for Microbial Diseases of Osaka University. Yuta Kunishima reports financial support was provided by The Research Foundation for Microbial Diseases of Osaka University. Chikako Kataoka-Nakamura reports financial support was provided by The Research Foundation for Microbial Diseases of Osaka University. Kota Senpuku reports financial support was provided by The Japan Science and Technology Agency. If there are other authors, they declare that they have no known competing financial interests or personal relationships that could have appeared to influence the work reported in this paper.

Acknowledgments

We acknowledge Hiroko Omori (Core Instrumentation Facility, Research Institute for Microbial Diseases, The University of Osaka) for her support with the negative-stain TEM assessment. We also acknowledge the NGS core facility at the Research Institute for Microbial Diseases of The University of Osaka for their support with the next-generation sequencing analysis.

Appendix A. Supplementary data

Supplementary data to this article can be found online at https://doi.org/10.1016/j.vaccine.2025.127314.

Data availability

The data supporting the findings of this study are presented in this article. Further information and requests for resources and reagents should be directed to and fulfilled by Yasuo Yoshioka (y-yoshioka@-biken.osaka-u.ac.jp).

References

[1] Zell R, et al. ICTV virus taxonomy profile: Picornaviridae. J Gen Virol 2017;98:2421–2. https://doi.org/10.1099/jgv.0.000911.

[2] Baggen J, Thibaut HJ, Strating J, van Kuppeveld FJM. The life cycle of non-polio enteroviruses and how to target it. Nat Rev Microbiol 2018;16:368–81. https://doi.org/10.1038/s41579-018-0005-4.

[3] Elrick MJ, Pekosz A, Duggal P. Enterovirus D68 molecular and cellular biology and pathogenesis. J Biol Chem 2021;296:100317. https://doi.org/10.1016/j.jbc.2021.100317.

[4] Greninger AL, et al. A novel outbreak enterovirus D68 strain associated with acute flaccid myelitis cases in the USA (2012-14): a retrospective cohort study. Lancet Infect Dis 2015;15:671–82. https://doi.org/10.1016/S1473-3099(15)70093-9.

[5] Midgley CM, et al. Severe respiratory illness associated with a nationwide outbreak of enterovirus D68 in the USA (2014): a descriptive epidemiological investigation. Lancet Respir Med 2015;3:879–87. https://doi.org/10.1016/S2213-2600(15)00335-5.

[6] Holm-Hansen CC, Midgley SE, Fischer TK. Global emergence of enterovirus D68: a systematic review. Lancet Infect Dis 2016;16:e64–75. https://doi.org/10.1016/S1473-3099(15)00543-5.

[7] Messacar K, Abzug MJ, Dominguez SR. The emergence of enterovirus-D68. Microbiol Spectr 2016;4:105–19. https://doi.org/10.1128/microbiolspec.EI10-0018-2016.

[8] Messacar K, et al. Acute flaccid myelitis: a clinical review of US cases 2012-2015. Ann Neurol 2016;80:326–38. https://doi.org/10.1002/ana.24730.

[9] Kujawski SA, et al. Enterovirus D68-associated acute respiratory illness - new vaccine surveillance network, United States, July-October, 2017 and 2018. MMWR Morb Mortal Wkly Rep 2019;68:277–80. https://doi.org/10.15585/mmwr.mm6812a1.

[10] McLaren N, et al. Characteristics of patients with acute flaccid myelitis, United States, 2015-2018. Emerg Infect Dis 2020;26:212–9. https://doi.org/10.3201/eid2602.191453.

[11] Park SW, et al. Epidemiological dynamics of enterovirus D68 in the United States and implications for acute flaccid myelitis. Sci Transl Med 2021;13:eabd2400. https://doi.org/10.1126/scitranslmed.abd2400.

[12] Benschop KS, et al. Re-emergence of enterovirus D68 in Europe after easing the COVID-19 lockdown, September 2021. Euro Surveill 2021;26:2100998. https://doi.org/10.2807/1560-7917.ES.2021.26.45.2100998.

[13] Ma KC, et al. Increase in acute respiratory illnesses among children and adolescents associated with rhinoviruses and enteroviruses, including enterovirus D68 - United States, July-September 2022. MMWR Morb Mortal Wkly Rep 2022;71:1265–70. https://doi.org/10.15585/mmwr.mm7140e1.

[14] Zhang C, et al. A mouse model of enterovirus D68 infection for assessment of the efficacy of inactivated vaccine. Viruses 2018;10:58. https://doi.org/10.3390/v10020058.

[15] Sun S, et al. A neonatal mouse model of enterovirus D68 infection induces both interstitial pneumonia and acute flaccid myelitis. Antiviral Res 2019;161:108–15. https://doi.org/10.1016/j.antiviral.2018.11.013.

[16] Zheng H, et al. Single B cells reveal the antibody responses of rhesus macaques immunized with an inactivated enterovirus D68 vaccine. Arch Virol 2020;165:1777–89. https://doi.org/10.1007/s00705-020-04676-6.

[17] Raychoudhuri A, Naru AK, Kanubothula SR, Uddala R. Development of an experimental inactivated vaccine from Vero cell adapted enterovirus D68. Virus Res 2021;304:198528. https://doi.org/10.1016/j.virusres.2021.198528.

[18] Senpuku K, Kataoka-Nakamura C, Kunishima Y, Hirai T, Yoshioka Y. An inactivated whole-virion vaccine for enterovirus D68 adjuvanted with CpG ODN or AddaVax elicits potent protective immunity in mice. Vaccine 2024;42:2463–74. https://doi.org/10.1016/j.vaccine.2024.03.016.

[19] Aubrit F, et al. Cell substrates for the production of viral vaccines. Vaccine 2015;33:5905–12. https://doi.org/10.1016/j.vaccine.2015.06.110.

[20] Hooi YT, Balasubramaniam V. In vitro and in vivo models for the study of EV-D68 infection. Pathology 2023;55:907–16. https://doi.org/10.1016/j.pathol.2023.08.007.

[21] Kouraklis G, Triche TJ, Wesley R, Tsokos M. Myc oncogene expression and nude mouse tumorigenicity and metastasis formation are higher in alveolar than embryonal rhabdomyosarcoma cell lines. Pediatr Res 1999;45:552–8. https://doi.org/10.1203/00006450-199904010-00015.

[22] Guidance for industry. Characterization and qualification of cell substrates and other biological starting materials used in the production of viral vaccines for the prevention and treatment of infectious diseases. Biotechnol Law Rep 2006;25:697–723. https://doi.org/10.1089/blr.2006.25.697.

[23] Trent D, et al. WHO working group on technical specifications for manufacture and evaluation of dengue vaccines, Geneva, Switzerland, 11-12 may 2009. Vaccine 2010;28:8246–55. https://doi.org/10.1016/j.vaccine.2010.10.043.

[24] Demirden SF, Kimiz-Gebologlu I, Oncel SS. Animal cell lines as expression platforms in viral vaccine production: a post Covid-19 perspective. ACS Omega 2024;9:16904–26. https://doi.org/10.1021/acsomega.3c10484.

[25] Dotti S, et al. Transformation and Tumorigenicity testing of simian cell lines and evaluation of poliovirus replication. PloS One 2017;12:e0169391. https://doi.org/10.1371/journal.pone.0169391.

[26] Oberste MS, et al. Enterovirus 68 is associated with respiratory illness and shares biological features with both the enteroviruses and the rhinoviruses. J Gen Virol 2004;85:2577–84. https://doi.org/10.1099/vir.0.79925-0.

[27] Ma B, et al. Characteristics and viral propagation properties of a new human diploid cell line, Walvax-2, and its suitability as a candidate cell substrate for vaccine production. Hum Vaccin Immunother 2015;11:998–1009. https://doi.org/10.1080/21645515.2015.1009811.

[28] Desmyter J, Melnick JL, Rawls WE. Defectiveness of interferon production and of rubella virus interference in a line of African green monkey kidney cells (Vero). J Virol 1968;2:955–61. https://doi.org/10.1128/JVI.2.10.955-961.1968.

[29] Emeny JM, Morgan MJ. Regulation of the interferon system: evidence that Vero cells have a genetic defect in interferon production. J Gen Virol 1979;43:247–52. https://doi.org/10.1099/0022-1317-43-1-247.

[30] Osada N, et al. The genome landscape of the african green monkey kidney-derived vero cell line. DNA Res 2014;21:673–83. https://doi.org/10.1093/dnares/dsu029.

[31] Smee DF, Evans WJ, Nicolaou KC, Tarbet EB, Day CW. Susceptibilities of enterovirus D68, enterovirus 71, and rhinovirus 87 strains to various antiviral compounds. Antiviral Res 2016;131:61–5. https://doi.org/10.1016/j.antiviral.2016.04.003.

[32] Wei W, et al. ICAM-5/Telencephalin is a functional entry receptor for enterovirus D68. Cell Host Microbe 2016;20:631–41. https://doi.org/10.1016/j.chom.2016.09.013.

[33] Kärber G. Beitrag zur kollektiven Behandlung pharmakologischer Reihenversuche. Arch Exp Pathol Pharmakol 1931;162:480–3. https://doi.org/10.1007/BF01863914.

[34] Liu Y, et al. Sialic acid-dependent cell entry of human enterovirus D68. Nat Commun 2015;6:8865. https://doi.org/10.1038/ncomms9865.

[35] Baggen J, et al. Enterovirus D68 receptor requirements unveiled by haploid genetics. Proc Natl Acad Sci U S A 2016;113:1399–404. https://doi.org/10.1073/pnas.1524498113.

[36] Baggen J, et al. Bypassing pan-enterovirus host factor PLA2G16. Nat Commun 2019;10:3171. https://doi.org/10.1038/s41467-019-11256-z.

[37] Tseligka ED, et al. A VP1 mutation acquired during an enterovirus 71 disseminated infection confers heparan sulfate binding ability and modulates ex vivo tropism. PLoS Pathog 2018;14:e1007190. https://doi.org/10.1371/journal.ppat.1007190.

[38] Rudy MJ, Coughlan C, Hixon AM, Clarke P, Tyler KL. Density analysis of enterovirus D68 shows viral particles can associate with exosomes. Microbiol Spectr 2022;10:e0245221. https://doi.org/10.1128/spectrum.02452-21.

[39] Rajput C, et al. Enterovirus D68 infection induces IL-17-dependent neutrophilic airway inflammation and hyperresponsiveness. JCI Insight 2018;3:e121882. https://doi.org/10.1172/jci.insight.121882.

[40] Kobayashi K, Mizuta K, Koike S. Heparan sulfate attachment receptor is a major selection factor for attenuated enterovirus 71 mutants during cell culture adaptation. PLoS Pathog 2020;16:e1008428. https://doi.org/10.1371/journal.ppat.1008428.

[41] Ayudhya Sooksawasdi Na, S., et al. Enhanced enterovirus D68 replication in neuroblastoma cells is associated with a cell culture-adaptive amino acid substitution in VP1. mSphere 2020;5:e00941. https://doi.org/10.1128/mSphere.00941-20.

[42] Vicente-Fermin O, et al. Effect of dexamethasone on the expression of the alpha2,3 and alpha2,6 sialic acids in epithelial cell lines. Pathogens 2022;11:1518. https://doi.org/10.3390/pathogens11121518.

[43] Hixon AM, Clarke P, Tyler KL. Contemporary circulating enterovirus D68 strains infect and undergo retrograde axonal transport in spinal motor neurons independent of sialic acid. J Virol 2019;93:e00578–619. https://doi.org/10.1128/JVI.00578-19.

[44] Rosenfeld AB, Warren AL, Racaniello VR. Neurotropism of enterovirus D68 isolates is independent of sialic acid and is not a recently acquired phenotype. mBio 2019;10:e02370–419. https://doi.org/10.1128/mBio.02370-19.

[45] Elrick MJ, Pekosz A, Duggal P. Correction: enterovirus D68 molecular and cellular biology and pathogenesis. J Biol Chem 2021;296:100587. https://doi.org/10.1016/j.jbc.2021.100587.

[46] Grizer CS, Messacar K, Mattapallil JJ. Enterovirus-D68 - a reemerging non-polio enterovirus that causes severe respiratory and neurological disease in children. Front Virol 2024;4:1328457. https://doi.org/10.3389/fviro.2024.1328457.

[47] Liu X, et al. MFSD6 is an entry receptor for respiratory enterovirus D68. Cell Host Microbe 2025;33. https://doi.org/10.1016/j.chom.2024.12.015. 267-278 e264.

[48] Varanese L, et al. MFSD6 is an entry receptor for enterovirus D68. Nature 2025. https://doi.org/10.1038/s41586-025-08908-0.

[49] Filipe IC, Guedes MS, Zdobnov EM, Tapparel C. Enterovirus D: a small but versatile species. Microorganisms 2021;9:1758. https://doi.org/10.3390/microorganisms9081758.

[50] Xia X, et al. Functions of Viroporins in the viral life cycle and their regulation of host cell responses. Front Immunol 2022;13:890549. https://doi.org/10.3389/fimmu.2022.890549.

[51] Lin YC, Wu CN, Shih SR, Ho MS. Characterization of a Vero cell-adapted virulent strain of enterovirus 71 suitable for use as a vaccine candidate. Vaccine 2002;20:2485–93. https://doi.org/10.1016/s0264-410x(02)00182-2.

[52] Chang JY, et al. Selection and characterization of vaccine strain for enterovirus 71 vaccine development. Vaccine 2012;30:703–11. https://doi.org/10.1016/j.vaccine.2011.11.087.
[53] Wu XX, et al. Process optimization for the rapid production of enterovirus 71. Cytotechnology 2019;71:1053–61. https://doi.org/10.1007/s10616-019-00340-3.
[54] Hu G, et al. Efficacy of Coxsackievirus A2 vaccine candidates correlating to humoral immunity in mice challenged with a mouse-adapted strain. Vaccine 2022;40:4716–25. https://doi.org/10.1016/j.vaccine.2022.06.021.
[55] Sun YS, et al. Development and evaluation of an inactivated coxsackievirus A16 vaccine in gerbils. Emerg Microbes Infect 2022;11:1994–2006. https://doi.org/10.1080/22221751.2022.2093132.
[56] Dai W, Li X, Liu Z, Zhang C. Identification of four neutralizing antigenic sites on the enterovirus D68 capsid. J Virol 2023;97:e0160023. https://doi.org/10.1128/jvi.01600-23.
[57] Liu Y, et al. Molecular basis for the acid-initiated uncoating of human enterovirus D68. Proc Natl Acad Sci U S A 2018;115:E12209–17. https://doi.org/10.1073/pnas.1803347115.
[58] Vogt MR, Crowe Jr JE. Current understanding of humoral immunity to enterovirus D68. J Pediatric Infect Dis Soc 2018;7:S49–53. https://doi.org/10.1093/jpids/piy124.
[59] Krug PW, et al. EV-D68 virus-like particle vaccines elicit cross-clade neutralizing antibodies that inhibit infection and block dissemination. Sci Adv 2023;9:eadg6076. https://doi.org/10.1126/sciadv.adg6076.
[60] Swain SK, Gadnayak A, Mohanty JN, Sarangi R, Das J. Does enterovirus 71 urge for effective vaccine control strategies? Challenges and current opinion. Rev Med Virol 2022;32:e2322. https://doi.org/10.1002/rmv.2322.
[61] Khoshnood S, et al. An overview on inactivated and live-attenuated SARS-CoV-2 vaccines. J Clin Lab Anal 2022;36:e24418. https://doi.org/10.1002/jcla.24418.
[62] Dadras O, et al. Safety and adverse events related to inactivated COVID-19 vaccines and Novavax;a systematic review. Arch Acad Emerg Med 2022;10:e54. https://doi.org/10.22037/aaem.v10i1.1585.
[63] Dyrdak R, et al. Outbreak of enterovirus D68 of the new B3 lineage in Stockholm, Sweden, august to September 2016. Euro Surveill 2016;21:30403. https://doi.org/10.2807/1560-7917.ES.2016.21.46.30403.
[64] Piralla A, et al. Enterovirus-D68 (EV-D68) in pediatric patients with respiratory infection: the circulation of a new B3 clade in Italy. J Clin Virol 2018;99-100:91–6. https://doi.org/10.1016/j.jcv.2018.01.005.
[65] Sun J, Hu XY, Yu XF. Current understanding of human enterovirus D68. Viruses 2019;11:490. https://doi.org/10.3390/v11060490.
[66] Midgley SE, et al. Co-circulation of multiple enterovirus D68 subclades, including a novel B3 cluster, across Europe in a season of expected low prevalence, 2019/20. Euro Surveill 2020;25:1900749. https://doi.org/10.2807/1560-7917.ES.2020.25.2.1900749.